# Odderon Effects in pp Collisions: Predictions for LHC Energies

**C. Merino*, M. M. Ryzhinskiy**, and Yu. M. Shabelski****

* **Departamento de Física de Partículas, Facultade de Física, and Instituto Galego de Física de Altas Enerxías (IGFAE), Universidade de Santiago de Compostela, Santiago de Compostela 15782, Galiza, Spain**
**E-mail: merino@fpaxp1.usc.es**

** **Petersburg Nuclear Physics Institute, Gatchina, St.Petersburg 188350, Russia**
**e-mail: mryzhinskiy@phmf.spbstu.ru**
**e-mail: shabelsk@thd.pnpi.spb.ru**

*Lecture given by Yu.M. Shabelski at the XLIII PNPI Winter School on Physics St.Petersburg, Russia*

*February 2009*

**A b s t r a c t**

We consider the possible contribution of Odderon (Reggeon with $\alpha_{Odd}(0) \sim 1$ and negative signature) exchange to the differences in the total cross sections of particle and antiparticle, to the ratios of real/imaginary parts of the elastic $pp$ amplitude, and to the differences in the inclusive spectra of particle and antiparticle in the central region. The experimental differences in total cross sections of particle and antiparticle are compatible with the existence of the Odderon component but such a large Odderon contribution seems to be inconsistent with the values of Re/Im ratios. In the case of inclusive particle and antiparticle production the current energies and/or accuracy of the experimental data don't allow a clear conclusion. It is expected that the LHC will finally solve the question of the Odderon existence.

# 1 Introduction

The Odderon is a singularity in the complex $J$-plane with intercept $\alpha_{Odd} \sim 1$, negative $C$-parity, and negative signature. Thus its zero flavour-number exchange contribution to particle-particle and to antiparticle-particle interactions, e.g., to $pp$ and $\bar{p}p$ total cross sections, has opposite signs. In QCD the Odderon singularity is connected [1] to the colour-singlet exchange of three reggeized gluons in $t$-channel. The theoretical and experimental status of Odderon has been recently discussed in refs. [2, 3]. The possibility to detect Odderon effects has also been investigated in other domains as $\pi p \to \rho N$ reaction [4], charm photoproduction [5], and diffractive production of pion pairs [6, 7].

The difference in the total cross sections of antiparticles and particles interactions with nucleon targets are numerically small and decrease rather fast with initial energy, so the Odderon coupling should be very small with respect to the Pomeron coupling. However, several experimental facts favouring the presence of the Odderon contribution exist. One of them is the difference in the $d\sigma/dt$ behaviour of elastic $pp$ and $\bar{p}p$ scattering at $\sqrt{s} = 52.8$ GeV and $|t| = 1 - 1.5$ GeV$^2$ presented in references [2, 8]. The behaviour of $pp$ and $\bar{p}p$ elastic scattering at ISR and SPS energies was analyzed in [9]. Also the differences in the yields of baryons and antibaryons produced in the central (midrapidity) region and in the forward hemisphere in meson-nucleon and in meson-nucleus collisions, and in the midrapidity region of high energy $pp$ interactions [10, 11, 12, 13, 14, 15, 16], can also be significant in this respect. The question of whether the Odderon exchange is needed for explaining these experimental facts, or they can be described by the usual exchange of a reggeized quark-antiquark pair with $\alpha_\omega(t) = \alpha_\omega(0) + \alpha'_\omega t$ ($\omega$-Reggeon exchange) is a fundamental one.

The detailed description of all available data on hadron-nucleon elastic scattering with accounting for Regge cuts results in $\alpha_\omega(0) = 0.43$, $\alpha'_\omega = 1$ GeV$^{-2}$ [17], and the simplest power fit

$$\Delta\sigma_{hp} \ = \sigma^{tot}_{\bar{h}p} - \sigma^{tot}_{hp} = \sigma_R \cdot (s/s_0)^{\alpha_R(0)-1} \tag{1}$$

for experimental points of $\bar{p}p$ and $pp$ scattering starting from $\sqrt{s} = 5$ GeV gives the value $\alpha_R = 0.424 \pm 0.015$ [18]. The accounting for Regge cut contributions of the type $RP$, $RPP$, $RP...P$, and $Rf$, $RfP$, $RfP...P$ slightly decrease (from $\alpha_R = 0.424 \pm 0.015$ to $\alpha_R = 0.364 \pm 0.015$) [18] the effective value of $\alpha_R$. Thus any process with exchange of a negative signature object with effective intercept $\alpha_{eff} > 0.7$ could be considered as an Odderon contribution, while if $\alpha_{eff} \leq 0.5$ one could say that there is no room for the Odderon contribution.

In this paper we carry out this anlysis for the case of high energy $hp$ collisions. In

Section 2 we study the Regge pole contributions from the data on $\bar{p}p$, $pp$, $\pi^{\pm}p$, and $K^{\pm}p$ total cross sections. In Section 3 we consider the possible Odderon effect on the ratios of real/imaginary parts of the elastic $pp$ amplitude. In Section 4 we compare the experimental ratios of $\bar{h}$ to $h$ inclusive production in the midrapidity (central) region for $pp$ collisions to predictions from double-Reggeon diagrams. In Sections 5, 6, and 7 we compare these experimental data to the theoretical predictions of the Quark–Gluon String Model (QGSM). Our predictions for the Odderon effects at LHC energies are presented in Section 8.

# 2 Regge-pole analysis of total $hp$ and $\bar{h}p$ cross sections

Let us start from the analysis of high energy elastic particle and antiparticle scattering on the proton target. Here the simplest contribution is the one Regge-pole $R$ exchange corresponding to the scattering amplitude

$$A(s,t) = g_1(t) \cdot g_2(t) \cdot \left(\frac{s}{s_0}\right)^{\alpha_R(t)-1} \cdot \eta(\Theta) \ , \tag{2}$$

where $g_1(t)$ and $g_2(t)$ are the couplings of a Reggeon to the beam and target hadrons, $\alpha_R(t)$ is the $R$-Reggeon trajectory, and $\eta(\Theta)$ is the signature factor which determines the complex structure of the scattering amplitude ($\Theta$ equal to $+1$ and to $-1$ for reggeon with positive and negative signature, respectively):

$$\eta(\Theta) = \begin{cases} i - \tan^{-1}(\frac{\pi\alpha_R}{2}) & \Theta = +1 \\ i + \tan(\frac{\pi\alpha_R}{2}) & \Theta = -1 \ , \end{cases} \tag{3}$$

so the amplitude $A(s, t = 0)$ becomes purely imaginary for positive signature and purely real for negative signature when $\alpha_R \to 1$.

The contribution of the Reggeon exchange with positive signature is the same for a particles and its antiparticle, but in the case of negative signature the two contributions have opposite signs, as it is shown in Fig. 1.

The difference in the total cross section of high energy particle and antiparticle scattering on the proton target is

$$\Delta\sigma_{hp}^{tot} = \sum_{R(\Theta=-1)} 2 \cdot Im\, A(s, t=0) = \sum_{R(\Theta=-1)} 2 \cdot g_1(0) \cdot g_2(0) \cdot \left(\frac{s}{s_0}\right)^{\alpha_R(0)-1} \cdot Im\, \eta(\Theta=-1) \ . \tag{4}$$

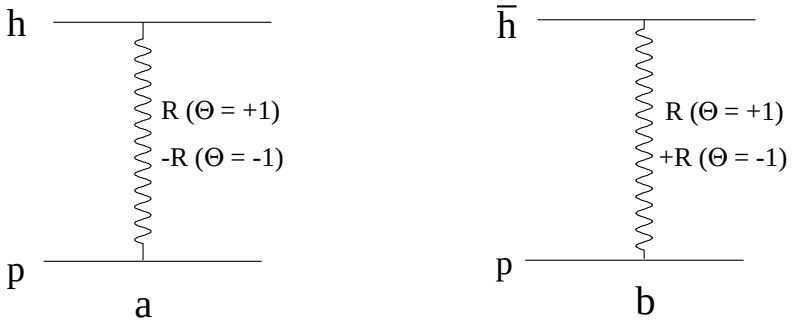


Figure 1: Diagram corresponding to the Reggeon-pole exchange in particle $h$ (a) (its antiparticle $\bar{h}$ (b)) interactions with a proton target. The positive signature ($\Theta = +1$) exchange contributions are the same, while the negative signature ($\Theta = -1$) exchange contributions have opposite signs.

The experimental data for the differences of $\bar{p}p$ and $pp$ total cross sections are presented in Fig. 2. Here we use the data compiled in ref. [19] by presenting at every energy the experimental points for $pp$ and $\bar{p}p$ by the same experimental group and with the smallest error bars. At ISR energies (last three points in Fig. 2) we present the data in ref. [20] as published in their most recent version.

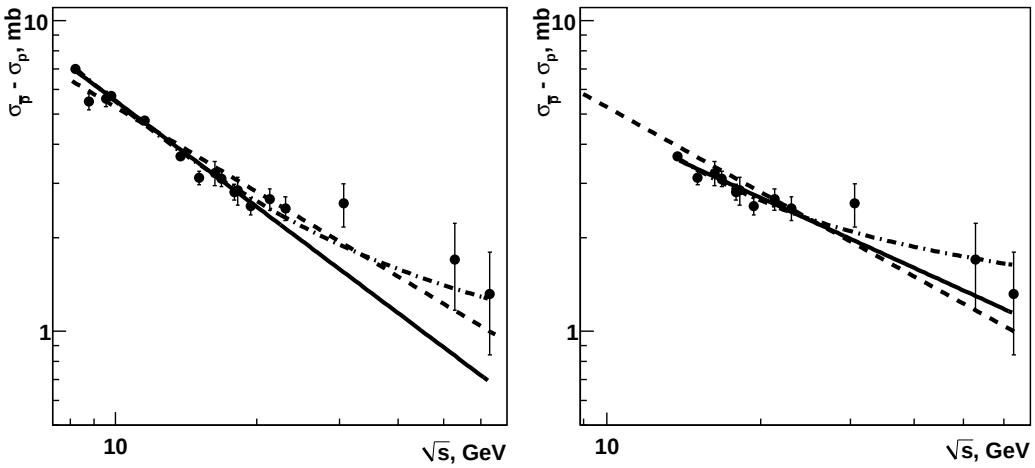


Figure 2: Experimental differences of $\bar{p}p$ and $pp$ total cross sections at $\sqrt{s} > 8$ GeV (left panel) and at $\sqrt{s} > 13$ GeV (right panel) together with their fit by Eq. (1) (solid curves), fit of [21] Eq. (5) (dashed curves) and fit by Eq. (6) (dash-dotted curves).

In the left panel of Fig. 2 our fit to the experimental data with Eq. (1) starting from $\sqrt{s} > 8$ GeV is presented (solid line). For this fit we obtain the value of $\alpha_R =$

$0.43 \pm 0.017$ with $\chi^2 = 33.3/15$ ndf. This result is in good agreement with [18], where the experimental points at energies $\sqrt{s} > 5$ GeV were included in the fit, and it only slightly differs from the general fit of all $hp$ total cross sections [21] which results in

$$\Delta\sigma_{pp} = 42.31 \cdot s^{-0.4525}(\text{mb}) \ , \tag{5}$$

and it starts from $\sqrt{s} > 10$ GeV. This last fit is also shown in Fig. 2 by a dashed line. The values of the parameters for the two fits, together with the $\chi^2$ values, are presented in Table 1. It is needed to note that the fit in [21] was aimed at the total $\bar{p}p$ and $pp$ cross sections and not specifically at their differences, so the not that good values of $\chi^2$ for this fit are not very significant.

As one can see in Table 1, the Eq. (1) fit can only describe the experimental difference in the total $\bar{p}p$ and $pp$ cross sections when starting from high enough energies. When starting at lower energies other Regge poles, as well as other contributions, can contribute, but their contribution becomes negligible at higher energies. Thus the values of the parameters in Eq. (1) can be different in different energy regions. To check the stability of the parameter values, we present in the right panel of Fig. 2 the same experimental data as in the left panel, but at $\sqrt{s} > 13$ GeV. Here we obtain $\alpha_R = 0.62 \pm 0.05$ with $\chi^2 = 8.3/10$ n.d.f., i.e. now the description of the data is better, with the value of $\alpha_R$ significantly increasing. This indicates that it is reasonable to account for two contributions to $\Delta\sigma_{pp}$, the first one corresponding to the well-known $\omega$-reggeon and the second one corresponding to a possible Odderon exchange:

$$\Delta\sigma_{hp} \ = \sigma_\omega \cdot (s/s_0)^{\alpha_\omega(0)-1} + \sigma_{Odd} \cdot (s/s_0)^{\alpha_{Odd}(0)-1} \ . \tag{6}$$

| Parameterization | $\sigma_R(mb)$ | $\alpha_R(0)$ | $\chi^2/ndf$ |
|---|---|---|---|
| $p^{\pm}p, \sqrt{s} > 8$ GeV (Eq. (1)) | $75.4 \pm 6.1$ | $0.43 \pm 0.017$ | 35.1/15 |
| $p^{\pm}p, \sqrt{s} > 13$ GeV (Eq. (1)) | $25.5 \pm 7.1$ | $0.625 \pm 0.05$ | 8.8/10 |
| $p^{\pm}p, \sqrt{s} > 8$ GeV (Eq. (5)) | 42.31 (fixed) | 0.5475 (fixed) | 92.3/17 |
| $p^{\pm}p, \sqrt{s} > 13$ GeV (Eq. (5)) | 42.31 (fixed) | 0.5475 (fixed) | 34.5/12 |
| $\pi^{\pm}p, \sqrt{s} > 8$ GeV (Eq. (1)) | $9.51 \pm 1.89$ | $0.51 \pm 0.04$ | 17.2/20 |
| $\pi^{\pm}p, \sqrt{s} > 8$ GeV (Eq. (5)) | 8.46 (fixed) | 0.5475 (fixed) | 26.3/22 |
| $K^{\pm}p, \sqrt{s} > 8$ GeV (Eq. (1)) | $28.0 \pm 3.7$ | $0.45 \pm 0.03$ | 15.4/18 |
| $K^{\pm}p, \sqrt{s} > 8$ GeV (Eq. (5)) | 8.46 (fixed) | 0.5475 (fixed) | 50.1/20 |

Table 1: The Regge-pole fits of the differences in $\bar{h}p$ and $hp$ total cross sections by using Eq. (1) and Eq. (5).

The accuracy of the available experimental points is not good enough for the determination of the values of the four parameters in Eq. (6), so by sticking to the idea

of existence of the Odderon, we have fixed the value of $\alpha_{Odd}(0)$ close to one (we take $\alpha_{Odd}(0) = 0.9$[1]), thus obtaining the fit shown by a dash-dotted curve both in the left panel and in the right panel of Fig. 2 with the values of the parameters presented in Table 2.

| Energy | $\sigma_\omega(mb)$ | $\alpha_\omega(0)$ | $\sigma_{Odd}(mb)$ | $\alpha_{Odd}(0)$ | $\chi^2$/ndf |
|---|---|---|---|---|---|
| $p^{\pm}p$, $\sqrt{s} > 8$ GeV | $165 \pm 37$ | $0.19 \pm 0.06$ | $2.65 \pm 0.45$ | 0.9 (fixed) | 26.7/14 |
| $p^{\pm}p$, $\sqrt{s} > 13$ GeV | $450 \pm 119$ | $-0.09 \pm 0.03$ | $3.61 \pm 0.09$ | 0.9 (fixed) | 5.8/9 |
| $p^{\pm}p$, $\sqrt{s} > 8$ GeV | $172 \pm 7$ | $0.15 \pm 0.09$ | $5.16 \pm 0.32$ | 0.8 (fixed) | 27.6/14 |
| $p^{\pm}p$, $\sqrt{s} > 13$ GeV | $450 \pm 164$ | $-0.16 \pm 0.05$ | $7.38 \pm 0.66$ | 0.8 (fixed) | 6.1/9 |
| $\pi^{\pm}p$, $\sqrt{s} > 8$ GeV | $20.8 \pm 42.6$ | $0.25 \pm 0.60$ | $0.52 \pm 0.69$ | 0.9 (fixed) | 16.7/19 |
| $K^{\pm}p$, $\sqrt{s} > 8$ GeV | $23. \pm 11.2$ | $0.52 \pm 0.86$ | $-0.55 \pm 1.72$ | 0.9 (fixed) | 15.3/17 |

Table 2: The double Regge-pole fit to the differences in $\bar{h}p$ and $hp$ total cross sections using Eq. (6).

From the results of this fit for $\sqrt{s} > 8$ GeV one can see that an Odderon contribution with $\alpha_{Odd}(0) \sim 0.9$ is in agreement with the experimental data, the values of $\chi^2$/ndf for parametrization by Eq. (6) being smaller that those in the case of Eq. (1). The contributions of Odderon and $\omega$-reggeon to the differences in $\bar{p}p$ and $pp$ total cross sections would be approximately equal at $\sqrt{s} \sim 25{-}30$ GeV. The fit with Eq. (6) at $\sqrt{s} > 13$ GeV qualitatively results in the same curve as the fit at $\sqrt{s} > 8$, but now the errors in the values of the parameters are very large.

Such large value of $\alpha_{Odd}(0)$ ($\alpha_{Odd}(0) \sim 0.9$) with a rather large Odderon coupling should necessarily reflect in a large value of the ratio

$$\rho = \frac{ReA(s, t = 0)}{ImA(s, t = 0)} \ , \tag{7}$$

but this could be in disagreement with the existing experimental data, as it will be discussed in the next section. In any case, this problem fades away when considering smaller values of $\alpha_{Odd}(0)$. For this reason in Table 2 we present our fits for the differences in $\bar{h}p$ and $hp$ total cross sections by using Eq. (6) with a fixed value $\alpha_{Odd}(0) = 0.8$. The new curves are very close to those of the $\alpha_{Odd}(0) = 0.9$ fit, but now the values of $\chi^2$/ndf are slightly increased.

In the left panel of Fig. 3 the experimental data for the differences of $\pi^- p$ and $\pi^+ p$ total cross sections taken from [19] are shown, together with the power fit of Eq. (1) (solid line), the fit in ref. [21] (dashed curve), and the double Reggeon fit of Eq. (6) with a value $\alpha_{Odd}(0) = 0.9$ (dash-dotted curve).

[1]The value of $\alpha_{Odd}(0)$ can *a priori* be larger than one.

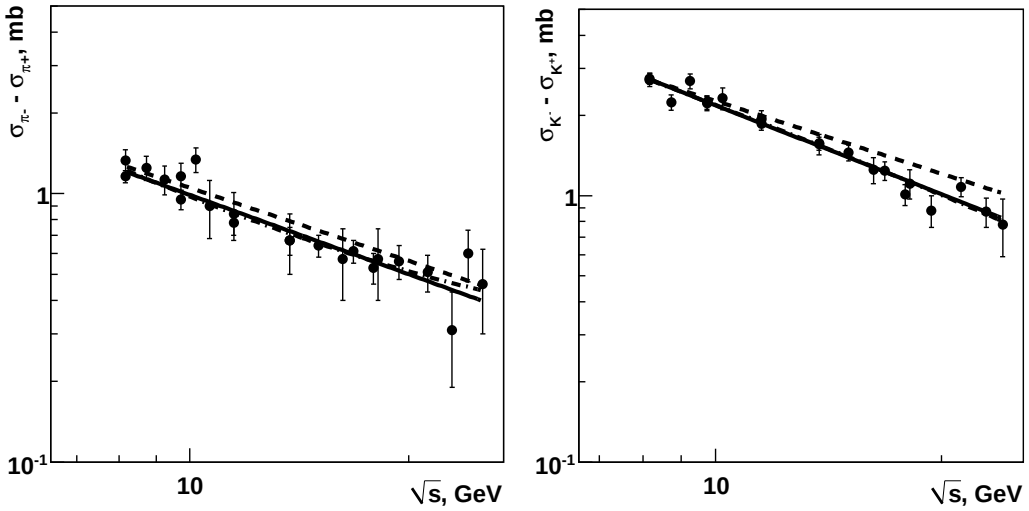


Figure 3: The experimental differences in $\pi^- p$ and $\pi^+ p$, left panel (and in $K^- p$ and $K^+ p$, right panel) total cross sections, together with their fits by Eq. (1) (solid curves), by ref. [21] (dashed curves), and by Eq. (6) (dash-dotted curves).

Since the Odderon corresponds to a three-gluon exchange, it can not contribute to the difference in $\pi^- p$ and $\pi^+ p$ total cross sections, what is consistent with our results, the values of $\chi^2$/ndf being practically the same for the solid and dash-dotted curves in Fig. 3, while the value of $\sigma_{Odd}$ is compatible with zero.

Similar results for the differences in $K^- p$ and $K^+ p$ total cross sections are shown in the right panel of Fig. 3. Here, the double Reggeon fit is again compatible with a zero Odderon contribution.

Needless to say, the presented results do not prove the Odderon existence in $pp$ scattering, We can only say that the assumption of the presence of an Odderon contribution is consistent with the experimental data on total $pp$ and $\bar{p}p$ cross sections. In any case, a more detailed analysis is needed, especially concerning the experimental error bars for the differences in $pp$ and $\bar{p}p$ cross sections. Thus, we have considered independent experimental values of the $pp$ and $\bar{p}p$ cross sections, but the experimental error bars in their differences would be decreased if both would be measured with the same experimental equipment.

# 3 Odderon contribution to the ratio Re/Im parts of elastic $pp$ amplitude

As one can see from Eqs. (2) and (3) the Odderon exchange generates a large real part of the elastic $pp$ amplitude which is proportional to $\tan(\frac{\pi\alpha_R}{2})$. The singularity at $\alpha_R = 1$ should be compensated by the smallness of the corresponding coupling. In the normalization, where $ImA_{hp} = \sigma^{tot}_{hp}$, one has

$$Re\,A_{Odd} = \frac{1}{2}(\sigma^{tot}_{\bar{p}p} - \sigma^{tot}_{pp})_{Odd} \cdot \tan\left(\frac{\pi\alpha_R}{2}\right) \ , \tag{8}$$

and the additional contribution by the Odderon to the total $\rho = ReA_{pp}/ImA_{pp}$ value it would be equal to

$$\rho_{Odd} = \frac{ReA_{Odd}}{\sigma^{tot}_{pp}} \ . \tag{9}$$

Results in Table 2 and in Fig. 2 show that the possible Odderon contribution to the difference in the total $pp$ and $\bar{p}p$ cross sections is of the order of the positive signature (mainly Pomeron) contribution at $\sqrt{s} \sim 25{-}30$ GeV and of about one half of the positive signature contribution at $\sqrt{s} \sim 10$ GeV. So, in the case of $\alpha_{Odd}(0) = 0.9$ the value of $ReA_{Odd}$ in Eq. (8) can be $ReA_{Odd} \sim$ 3-4 mb, what would result in an additional $\rho_{Odd} = 0.07$-$0.1$ contribution to the total $ReA_{pp}/ImA_{pp}$ ratio. This additional Odderon contribution would be in disagreement with the experimental data presented in Table 3.

In fact, the experimental data in refs. [22, 23] are in good agreement with the theoretical estimations based on the dispersion relations without Odderon contribution [24], so the hypothetical Odderon contribution could be as much of the order of the experimental error bars. The same situation appears at the CERN-SPS energy [25]. On the other hand, the experimental points [26, 27] allows some room for the presence of the Odderon contribution. It is necessary to keep in mind that the theoretical predictions also have some "error bars", e.g. the predictions for UA4 energy presented in [25] are between $\rho = 0.12$ [28] and $\rho = 0.15$ [29].

Let us note that the level of disagreement of the theoretical estimations on $\rho_{Odd}$ with experimental data decreases when decreasing the value of $\alpha_{Odd}$.

| Experiment | $\rho(s)$ | Theory |
|---|---|---|
| $\sqrt{s} = 13.7$ GeV [22] | $-0.092 \pm 0.014$ | $-0.085$ [24] |
| $\sqrt{s} = 13.7$ GeV [26] | $-0.074 \pm 0.018$ | $-0.085$ [24] |
| $\sqrt{s} = 15.3$ GeV [26] | $-0.024 \pm 0.014$ | $-0.060$ [24] |
| $\sqrt{s} = 16.8$ GeV [22] | $-0.040 \pm 0.014$ | $-0.047$ [24] |
| $\sqrt{s} = 16.8$ GeV [26] | $0.008 \pm 0.017$ | $-0.047$ [24] |
| $\sqrt{s} = 18.1$ GeV [26] | $-0.011 \pm 0.019$ | $-0.04$ [24] |
| $\sqrt{s} = 19.4$ GeV [26] | $0.019 \pm 0.016$ | $-0.033$ [24] |
| $\sqrt{s} = 21.7$ GeV [22] | $-0.041 \pm 0.014$ | $-0.02$ [24] |
| $\sqrt{s} = 23.7$ GeV [22] | $-0.028 \pm 0.016$ | $-0.007$ [24] |
| $\sqrt{s} = 30.6$ GeV [23] | $0.042 \pm 0.011$ | 0.03 [24] |
| $\sqrt{s} = 44.7$ GeV [23] | $0.062 \pm 0.011$ | 0.062 [24] |
| $\sqrt{s} = 52.9$ GeV [23] | $0.078 \pm 0.010$ | 0.075 [24] |
| $\sqrt{s} = 62.4$ GeV [23] | $0.095 \pm 0.011$ | 0.084 [24] |
| $\sqrt{s} = 546$ GeV [27] | $0.24 \pm 0.04$ | 0.10−0.15 [27] |
| $\sqrt{s} = 541$ GeV [25] | $0.135 \pm 0.015$ | 0.12−0.15 [28, 29] |

Table 3: Experimental data for the ratio Re/Im parts of elastic $pp$ amplitude at high energies together with the corresponding theoretical estimations.

# 4 Regge-pole analysis of inclusive particle and antiparticle production in the central region

The inclusive cross section of the production of a secondary $h$ in high energy $pp$ collisions in the central region is determined by the Regge-pole diagrams shown in Fig. 4 [30]. The diagram with only Pomeron exchange (Fig. 4a) is the leading one, while the diagrams with one secondary Reggeon $R$ (Figs. 4b and 4c) correspond to corrections which disappear with the increase of the initial energy.

The inclusive production cross section of hadron $h$ with transverse momentum $p_T$ corresponding to the diagram shown in Fig. 4b has the following expression:

$$F(p_T, s_1, s_2, s) = \frac{1}{\pi^2 s} g_R^{pp} \cdot g_P^{pp} \cdot g_{RP}^{hh}(p_T) \cdot \left(\frac{s_1}{s_0}\right)^{\alpha_R(0)} \cdot \left(\frac{s_2}{s_0}\right)^{\alpha_P(0)} , \tag{10}$$

where

$$\begin{aligned} s_1 &= (p_a + p_h)^2 = m_T \cdot s^{1/2} \cdot e^{-y^*} \\ s_2 &= (p_b + p_h)^2 = m_T \cdot s^{1/2} \cdot e^{y^*} , \end{aligned} \tag{11}$$

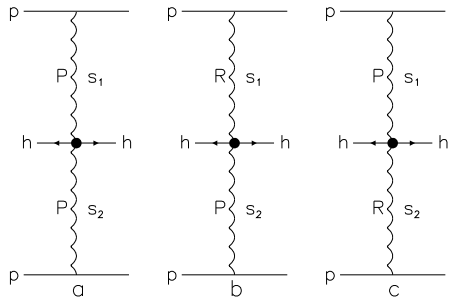


Figure 4: Regge-pole diagrams for the inclusive production of a secondary hadron $h$ in the central region.

with $s_1 \cdot s_2 = m_T^2 \cdot s$ [31], and the rapidity $y^*$ defined in the center-of-mass frame.

The contribution of diagram in Fig. 4c differs from Eq. (10) in the change of $s_1$ by $s_2$ and viceversa, and in the contribution of the diagram in Fig. 4a is obtained from Eq. (10) by changing the Reggeon $R$ by Pomeron $P$.

Let us consider the $R$-Reggeon in Fig. 4 as the effective sum of all amplitudes with negative signature, so its contribution to the inclusive spectra of secondary protons and antiprotons has the opposite sign. In the midrapidity region, i.e. at $y^* = 0$, the ratios ($\langle m_T \rangle \simeq 1$ GeV) of $p$ and $\bar{p}$ yields integrated over $p_T$ can be written as

$$\frac{\bar{p}}{p} = \frac{1 - r_-(s)}{1 + r_-(s)} \, , \tag{12}$$

where $r_-(s)$ is the ratio of the negative signature ($R$) to the positive signature ($P$) contributions:

$$r_-(s) = c_1 \cdot \left( \frac{s}{s_0} \right)^{(\alpha_R(0) - \alpha_P(0))/2} \, , \tag{13}$$

and $c_1$ is a normalization constant.

The theoretical fit by Eq. (12) to the experimental data [32, 33, 34, 35, 36, 37] on the ratios of $\bar{p}$ to $p$ production cross sections at $y^* = 0$ is presented in Fig. 5. Here we have used four experimental points from RHIC, obtained by BRAHMS, PHOBOS, PHENIX, and STAR Collaborations, and we present both $\bar{p}/p$ and $1 - \bar{p}/p$ as functions of initial energy. The obtained values of the parameters $c_1$ and $\alpha_R(0) - \alpha_P(0)$ are presented in Table 4.

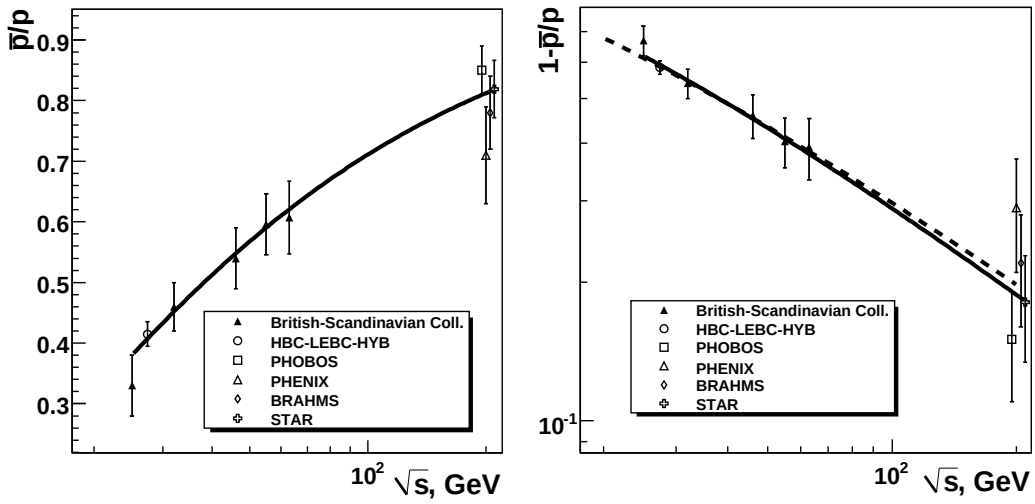


Figure 5: Ratios of $\bar{p}$ to $p$ production cross sections in high energy $pp$ collisions at $y^* = 0$, together with their fit by Eq. (12) (solid curves). Dashed curve shows the result of the fit with only the BRAHMS point at RHIC energy.

| Parameterization | $c_1$ | $\alpha_R(0) - \alpha_P(0)$ | $\chi^2$/ndf |
|---|---|---|---|
| $\bar{p}/p$ (Eq. (13), Fig. 5) | $4.4 \pm 1.1$ | $-0.71 \pm 0.07$ | 4.3/8 |
| $K^-/K^+$ (Eq. (13), Fig. 6) | $2.8 \pm 2.6$ | $-0.90 \pm 0.27$ | 2.0/8 |
| $\bar{p}/p$ (Eq. (14), Fig. 7) | $4.0 \pm 0.7$ | $-0.79 \pm 0.04$ | 15.0/8 |
| $K^-/K^+$ (Eq. (14), Fig. 7) | $2.3 \pm 0.8$ | $-0.99 \pm 0.12$ | 10.0/7 |
| $\pi^-/\pi^+$ (Eq. (14), Fig. 7) | $0.44 \pm 0.12$ | $-0.98 \pm 0.11$ | 34.5/7 |

Table 4: The Regge-pole fit of the experimental ratios of $\bar{h}p$ and $hp$ total cross sections by using Eqs. (12) and (13), and by using Eqs. (12) and (15).

The value of difference of $\alpha_R(0) - \alpha_P(0)$ obtained in the fit seems to be too large for allowing the presence of an Odderon contribution.

The corresponding fit of the experimental data [32, 33, 34, 35, 36, 37] on the ratios of $K^-$ to $K^+$ production cross sections at $y^* = 0$ is presented in Fig. 6, again for $K^-/K^+$ and $1-K^-/K^+$ as functions of the initial energy. The values of the parameters obtained in the fit are also presented in Table 3. The value of $\alpha_R(0) - \alpha_P(0)$ obtained in the $K^-/K^+$ is compatible with the value obatined in the $\bar{p}/p$ fit.

It is needed to note that both fits in Figs. (5) and (6) are in fact normalized to the experimental point in ref. [33], since the error bar of this point is several times smaller than those of the other considered experimental data.

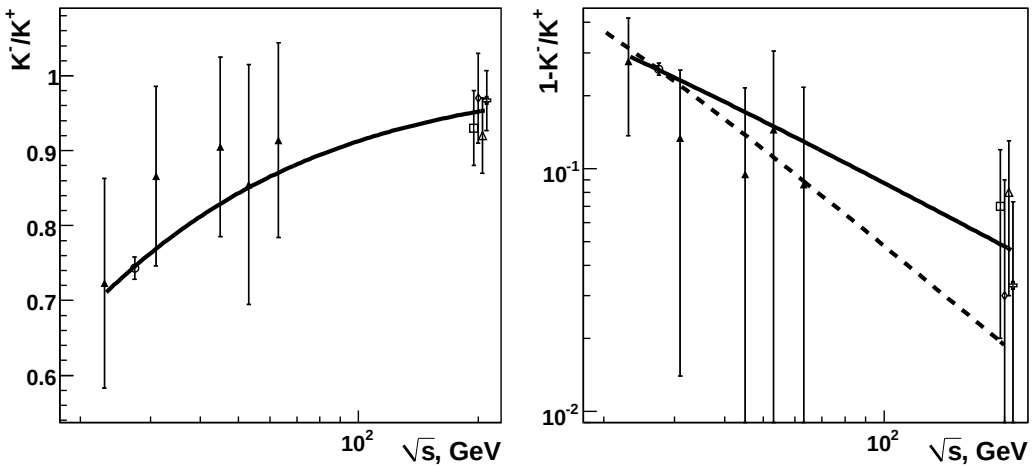


Figure 6: Ratios of $K^-$ to $K^+$ production cross sections in high energy $pp$ collisions at $y^* = 0$, together with their fit by Eq. (12) (solid curves). Dashed curve shows the result of the fit with only the BRAHMS point at RHIC energy.

The ratios of $\pi^-$ over $\pi^+$ production cross sections in midrapidity region $y^* = 0$ differ from unity only at moderate energies where different processes can contribute. At higher energies, where the applicability of Regge-pole asymptotics seems to be reasonable, these ratios are very close to one, so they can not be used in our analysis.

Though the experimental points for antiparticle/particle yield ratios obtained by different Collaborations at RHIC energy $\sqrt{s} = 200$ GeV are in reasonable agreement with each other (see Figs. 5 and 6), the BRAHMS Collaboration results [38] are of special interest because they were obtained not only at $y^* = 0$, but also at different values of non-zero rapidity $y^*$, and they can then provide some additional information.

Thus we present in the right panels of Figs. 5 and 6 the results of the fit to the same experimental data [32, 33] at $\sqrt{s} < 70$ GeV, but only considering BRAHMS Collaboration experimental point at RHIC energy (dashed curves). In the case of the $\bar{p}$ to $p$ ratio the result of this fit is practically the same as with all four RHIC points (solid curve in Fig. 5). However in the case of the $K^-$ to $K^+$ ratio the fit with only the BRAHMS Collaboration experimental point (dashed curve) significantly differs from the solid curve, meaning that the energy dependence of the $K^-$ to $K^+$ experimental ratio is very poorly known.

For the case of inclusive production at some rapidity distance $y^* \neq 0$ from the c.m.s. the quantitiy $r_-(s, y^*)$ in Eq. (12) takes the form:

$$r_-(s, y^*) = \frac{c_1}{2} \cdot \left(\frac{s}{s_0}\right)^{(\alpha_R(0)-\alpha_P(0))/2} \cdot \left(e^{y^*(\alpha_R(0)-\alpha_P(0))} + e^{-y^*(\alpha_R(0)-\alpha_P(0))}\right) . \qquad (14)$$

In Fig. 7 we present the fit to the experimental rapidity distribution ratios $\bar{p}/p$ (left panel), $K^-/K^+$ (right panel), and $\pi^-/\pi^+$ (lower panel) at $\sqrt{s} = 200$ GeV [34] by using Eq. (14). The values of parameters obtained in this fit are in agreement with those in the fits of Figs. 5 and 6 (see Table 3), so we can arguably claim that in the framework of Regge-pole phenomenology one gets a model independent description of the rapidity dependence of the $\bar{p}/p$ and $K^-/K^+$ ratios by using the values of the parameters that were obtained in the description of the energy dependence of these ratios at $y^* = 0$ using Eq. (12).

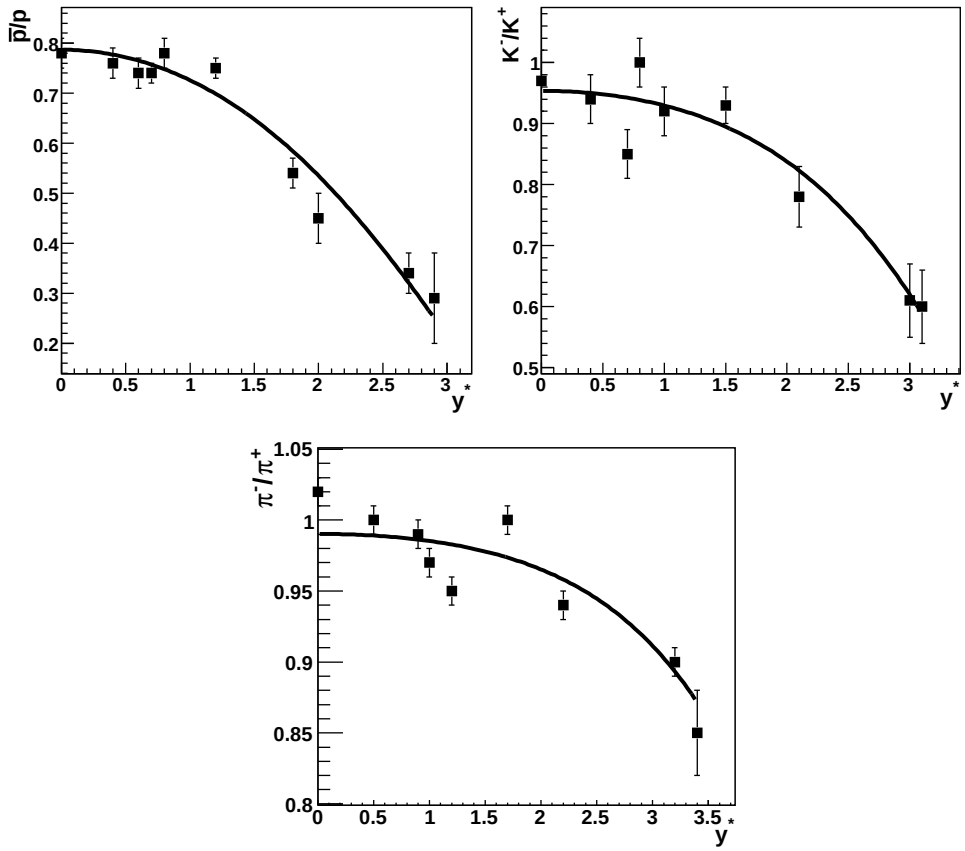


Figure 7: Ratios of the inclusive cross sections $\bar{p}$ to $p$ (left panel), $K^-$ to $K^+$ (right panel), and $\pi^-$ to $\pi^+$ (lower panel) in $pp$ collisions at $\sqrt{s} = 200$ GeV [34] as function of the c.m. rapidity, together with their fit by Eq. (14) (solid curves).

The values of $\alpha_R(0) - \alpha_P(0)$ for the $K^-/K^+$ and $\pi^-/\pi^+$ ratios are the same and they seem to be larger than the value for the $\bar{p}/p$ ratio. This situation is qualitatively similar to that of the differences in the total cross sections considered in Section 2.

However, the fit $\bar{p}/p$ ratios provide values of $\alpha_R(0) - \alpha_P(0)$ significantly larger than those one could expect if the Odderon contribution was present.

# 5 Inclusive spectra of secondary hadrons in the Quark-Gluon String Model

The ratios of inclusive production of different secondaries can also be analyzed in the framework of the Quark-Gluon String Model (QGSM) [39, 40, 41], which allows us to make quantitative predictions at different rapidities including the target and beam fragmentation regions. In QGSM high energy hadron-nucleon collisions are considered as taking place via the exchange of one or several Pomerons, all elastic and inelastic processes resulting from cutting through or between Pomerons [42].

Each Pomeron corresponds to a cylindrical diagram (see Fig. 8a), and thus, when cutting one Pomeron, two showers of secondaries are produced as it is shown in Fig. 8b. The inclusive spectrum of a secondary hadron $h$ is then determined by the convolution of the diquark, valence quark, and sea quark distributions $u(x, n)$ in the incident particles with the fragmentation functions $G^h(z)$ of quarks and diquarks into the secondary hadron $h$. These distributions, as well as the fragmentation functions are constructed using the Reggeon counting rules [43]. Both the diquark and the quark distribution functions depend on the number $n$ of cut Pomerons in the considered diagram.

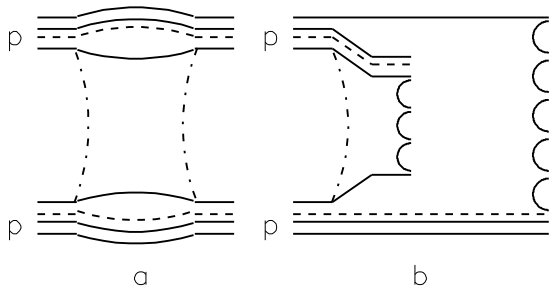


Figure 8: Cylindrical diagram corresponding to the one–Pomeron exchange contribution to elastic $pp$ scattering (a), and the cut of this diagram which determines the contribution to the inelastic $pp$ cross section (b). Quarks are shown by solid curves and string junction by dashed curves.

For a nucleon target, the inclusive rapidity or Feynman-$x$ ($x_F$) spectrum of a sec-

ondary hadron $h$ has the form [39]:

$$\frac{dn}{dy} \;=\; \frac{x_E}{\sigma_{inel}} \cdot \frac{d\sigma}{dx_F} \;=\; \sum_{n=1}^{\infty} w_n \cdot \phi_n^h(x) \;, \tag{15}$$

where the functions $\phi_n^h(x)$ determine the contribution of diagrams with $n$ cut Pomerons and $w_n$ is the relative weight of this diagram. Here we neglect the contribution of diffraction dissociation processes which is very small in the midrapidity region.

For $pp$ collisions

$$\begin{aligned} \phi_{pp}^h(x) \;&=\; f_{qq}^h(x_+,n) \cdot f_q^h(x_-,n) + f_q^h(x_+,n) \cdot f_{qq}^h(x_-,n) \\ &\qquad + 2(n-1) f_s^h(x_+,n) \cdot f_s^h(x_-,n) \;, \end{aligned} \tag{16}$$

$$x_\pm \;=\; \frac{1}{2}\left[\sqrt{4m_T^2/s + x^2} \;\pm x\right], \tag{17}$$

where $f_{qq}$, $f_q$, and $f_s$ correspond to the contributions of diquarks, valence quarks, and sea quarks, respectively.

These functions are determined by the convolution of the diquark and quark distributions with the fragmentation functions, e.g. for the quark one can write:

$$f_q^h(x_+,n) \;=\; \int_{x_+}^{1} u_q(x_1,n) \cdot G_q^h(x_+/x_1) dx_1 \;. \tag{18}$$

The diquark and quark distributions, which are normalized to unity, as well as the fragmentation functions, are determined by the corresponding Regge intercepts [43].

At very high energies both $x_+$ and $x_-$ are negligibly small in the midrapidity region and all fragmentation functions, which are usually written [43] as $G_q^h(z) = a_h(1-z)^\beta$, become constants that are equal for a particle and its antiparticle (this would correspond to the limit $r_-(s) \to 0$ in Eq. (12)):

$$G_q^h(x_+/x_1) = a_h \;. \tag{19}$$

This leads, in agreement with [30], to

$$\frac{dn}{dy} \;=\; g_h \cdot (s/s_0)^{\alpha_P(0)-1} \sim a_h^2 \cdot (s/s_0)^{\alpha_P(0)-1} \,, \tag{20}$$

that corresponds to the only one-Pomeron exchange diagram in Fig. 4a, the only diagram contributing to the inclusive density in the central region (AGK theorem [42]) at asymptotically high energy. The intercept of the supercritical Pomeron $\alpha_P(0) = 1+\Delta$, $\Delta = 0.139$ [41], is used in the QGSM numerical calculations.

# 6 The baryon as a 3q+SJ system

In the string models, baryons are considered as configurations consisting of three connected strings (related to three valence quarks) called string junction (SJ) [44, 45, 46, 47]. The colour part of a baryon wave function reads as follows [44, 46] (see Fig. 9):

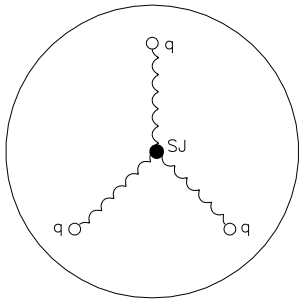


Figure 9: The composite structure of a baryon in string models. Quarks are shown by open points.

$$B = \psi_i(x_1) \cdot \psi_j(x_2) \cdot \psi_k(x_3) \cdot J^{ijk}(x_1, x_2, x_3, x)\,, \tag{21}$$

$$J^{ijk}(x_1, x_2, x_3, x) = \Phi^i_{i'}(x_1, x) \cdot \Phi^j_{j'}(x_2, x) \cdot \Phi^k_{k'}(x_3, x) \cdot \epsilon^{i'j'k'}\,, \tag{22}$$

$$\Phi^{i'}_i(x_1, x) = \left[ T \cdot \exp\left( g \cdot \int\limits_{P(x_1,x)} A_\mu(z) dz^\mu \right) \right]^{i'}_i\,, \tag{23}$$

where $x_1, x_2, x_3$, and $x$ are the coordinates of valence quarks and SJ, respectively, and $P(x_1, x)$ represents a path from $x_1$ to $x$ which looks like an open string with ends at $x_1$ and $x$. Such a baryon structure is supported by lattice calculations [48].

This picture leads to some general phenomenological predictions. In particular, it opens room for exotic states, such as the multiquark bound states, 4-quark mesons, and pentaquarks [46, 49, 50]. In the case of inclusive reactions the baryon number transfer to large rapidity distances in hadron-nucleon and hadron-nucleus reactions can be explained [10, 11, 12, 13, 14, 15] by SJ diffusion.

The production of a baryon-antibaryon pair in the central region usually occurs via $SJ$-$\overline{SJ}$ (according to Eqs. (21) and (22) SJ has upper color indices, whereas antiSJ ($\overline{SJ}$) has lower indices) pair production which then combines with sea quarks and sea

antiquarks into, respectively, $B\bar{B}$ pair [46, 51], as it is shown in Fig. (10). In the case of $pp$ collisions the existence of two SJ in the initial state and their diffusion in rapidity space lead to significant differences in the yields of baryons and antibaryons in the midrapidity region even at rather high energies [10, 12].

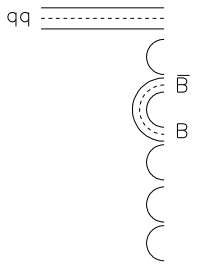


Figure 10: Diagram corresponding to the diquark fragmentation function for the production of a central $\bar{B}B$ pair. Quarks are shown by solid curves and SJ by dashed curves.

The quantitative theoretical description of the baryon number transfer via SJ mechanism was suggested in the 90's and used to predict [52] the $p/\bar{p}$ asymmetry at HERA energies then experimentally observed [53]. Also in ref. [54] was noted that the $p/\bar{p}$ asymmetry measured at HERA can be obtained by simple extrapolation of ISR data. The quantitative description of the baryon number transfer due to SJ diffusion in rapidity space was obtained in [10] and following papers [10, 11, 12, 13, 14, 15, 16].

In the QGSM the differences in the spectra of secondary baryons and antibaryons produced in the central region appear for processes which present SJ diffusion in rapidity space. These differences only vanish rather slowly when the energy increases.

To obtain the net baryon charge, and according to ref. [10], we consider three different possibilities. The first one is the fragmentation of the diquark giving rise to a leading baryon (Fig. 11a). A second possibility is to produce a leading meson in the first break-up of the string and a baryon in a subsequent break-up [43, 55] (Fig. 11b). In these two first cases the baryon number transfer is possible only for short distances in rapidity. In the third case, shown in Fig. 11c, both initial valence quarks recombine with sea antiquarks into mesons $M$ while a secondary baryon is formed by the SJ together with three sea quarks.

The fragmentation functions for the secondary baryon $B$ production corresponding to the three processes shown in Fig. 11 can be written as follows (see [10] for more details):

$$G^B_{qq}(z) \;\; = \;\; a_N \cdot v_{qq} \cdot z^{2.5} \; , \tag{24}$$

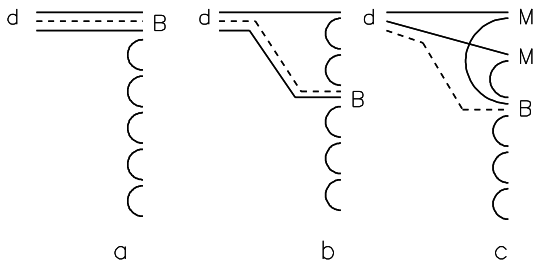


Figure 11: QGSM diagrams describing secondary baryon $B$ production by diquark $d$: initial SJ together with two valence quarks and one sea quark (a), initial SJ together with one valence quark and two sea quarks (b), and initial SJ together with three sea quarks (c).

$$G^B_{qs}(z) = a_N \cdot v_{qs} \cdot z^2 \cdot (1-z) \, , \tag{25}$$

$$G^B_{ss}(z) = a_N \cdot \varepsilon \cdot v_{ss} \cdot z^{1-\alpha_{SJ}} \cdot (1-z)^2 \, , \tag{26}$$

for Figs. 11a, 11b, and 11c, respectively, and where $a_N$ is the normalization parameter, and $v_{qq}$, $v_{qs}$, $v_{ss}$ are the relative probabilities for different baryons production that can be found by simple quark combinatorics [56, 57].

The fraction $z$ of the incident baryon energy carried by the secondary baryon decreases from Fig. 11a to Fig. 11c, whereas the mean rapidity gap between the incident and secondary baryon increases. The first two processes can not contribute to the inclusive spectra in the central region, but the third contribution is essential if the value of the intercept of the SJ exchange Regge-trajectory, $\alpha_{SJ}$, is large enough. At this point it is important to stress that since the quantum number content of the $SJ$ exchange matches that of the possible Odderon exchange, if the value of the $SJ$ Regge-trajectory intercept, $\alpha_{SJ}$, would turn out to be large and it would coincide with the value of the Odderon Regge-trajectory, $\alpha_{SJ} \simeq 0.9$, then the $SJ$ could be identified to the Odderon, or to one baryonic Odderon component.

Let's finally note that the process shown in Fig. 11c can be very naturally realized in the quark combinatorial approach [56] through the specific probabilities of a valence quark recombination (fusion) with sea quarks and antiquarks, the value of $\alpha_{SJ}$ depending on these specific probabilities.

The contribution of the graph in Fig. 11c has in QGSM a coefficient $\varepsilon$ which determines the small probability for such a baryon number transfer to occur.

At high energies the SJ contribution from Eq. (26) to the inclusive cross section of secondary baryon production at large rapidity distance $\Delta y$ from the incident nucleon

can be estimated as

$$\frac{1}{\sigma}\cdot\frac{d\sigma^B}{dy}\sim a_B\cdot\varepsilon\cdot e^{(1-\alpha_{SJ})\Delta y}\,, \tag{27}$$

where $a_B = a_N\cdot v_{ss}^B$. The baryon charge transferred to large rapidity distances can be determined by integration of Eq. (27), so being of the order of

$$\langle n_B\rangle\sim\frac{a_B\cdot\varepsilon}{(1-\alpha_{SJ})}\,. \tag{28}$$

It is then clear that the value $\alpha_{SJ}\geq 1$ should be excluded due to the violation of baryon-number conservation at asymptotically high energies.

# 7 Comparison of the QGSM predictions to the experimental data

With the value $\alpha_{SJ}=0.5$ used to obtain the first QGSM predictions [10] different values of $\varepsilon$ in Eq. (26) were needed for the correct description of the experimental data at moderate and high energies. A better solution was found in ref. [11], where it was shown that all experimental data can be described with the value $\alpha_{SJ}=0.9$ and only one value of $\varepsilon$. This large value of $\alpha_{SJ}$ allows to describe the preliminary experimental data of H1 Collaboration [53] on asymmetry of $p$ and $\bar{p}$ production in $\gamma p$ interactions at HERA with a rather small change in the description of the data at moderate energies. A similar analysis presented in ref. [13] for midrapidity asymmetries of $\bar{\Lambda}/\Lambda$ produced in $pp$, $pA$, $\pi p$, and $ep$ interactions also shows that the value $\alpha_{SJ}=0.9$ is slightly favoured, mainly due to the H1 Collaboration point [58].

Here we compare the results of QGSM predictions with all available experimental data on the $\bar{p}/p$ ratios presented in Fig. 5. To obtain these predictions we use the values of the probabilities $w_n$ in Eq. (15) that are calculated in the frame of Reggeon theory [39], and the values of the normalization constants $a_\pi$ (pion production), $a_K$ (kaon production), $a_{\bar{N}}$ ($B\bar{B}$ pair production), and $a_N$ (baryon production due to SJ diffusion) that were determined [39, 40, 41] from the experimental data at fixed target energies.

To compare the QGSM results obtained with different values of $\alpha_{SJ}$ in Eq. (26) all curves should be normalized at the same arbitrary point. This can be done in two different ways, either to use the experimental points at the highest energy, or to use the experimental point with the smallest error bar.

In the first case one takes into account that Reggeon theory is an asymptotic theory, and so numerically small (say of the order of 10%) disagreements with the experimental

data at fixed target energies are not very important. This first possibility was used in [11, 15] to obtain a rather good description of high energy data (HERA, RHIC, and ISR), and a reasonable agreement with the data at fixed target energies. However, the value of $\chi^2$ calculated here from the data at fixed target energies is not that good.

As example we present in Table 5 the calculated yields of different secondaries produced in $pp$ collisions at RHIC energy $\sqrt{s} = 200$ GeV [15].

| Particle | RHIC ($\sqrt{s} = 200$ GeV) | | |
|---|---|---|---|
| | $\varepsilon = 0$ | $\varepsilon = 0.024$ | STAR Collaboration [59] |
| $\pi^+$ | 1.27 | | |
| $\pi^-$ | 1.25 | | |
| $K^+$ | 0.13 | | $0.14 \pm 0.01$ |
| $K^-$ | 0.12 | | $0.14 \pm 0.01$ |
| $p$ | 0.0755 | 0.0861 | |
| $\overline{p}$ | 0.0707 | | |
| $\Lambda$ | 0.0328 | 0.0381 | $0.0385 \pm 0.0035$ |
| $\overline{\Lambda}$ | 0.0304 | | $0.0351 \pm 0.0032$ |
| $\Xi^-$ | 0.00306 | 0.00359 | $0.0026 \pm 0.0009$ |
| $\overline{\Xi}^+$ | 0.00298 | | $0.0029 \pm 0.001$ |
| $\Omega^-$ | 0.00020 | 0.00025 | * |
| $\overline{\Omega}^+$ | 0.00020 | | * |

*$dn/dy(\Omega^- + \overline{\Omega}^+) = 0.00034 \pm 0.00019$

Table 5: The QGSM results ($\alpha_{SJ} = 0.9$) for midrapidity yields $dn/dy$ ($|y| < 0.5$) integrated over $p_T$ for different secondaries at RHIC energies. The results for $\varepsilon = 0.024$ are presented only when different from the case $\varepsilon = 0$.

The second way was used in [16], where it was possible to describe all the data with good $\chi^2$, except for the $\bar{p}p$ and $\bar{\Lambda}\Lambda$ asymmetries at HERA (see discussion below). In this case the experimental value of $\bar{p}/p$ ratio at $\sqrt{s} = 27.4$ GeV [33] was chosen as normalization. To do so it was necessary to slightly change the fragmentation function of $uu$ and $ud$ diquarks into secondary antiproton, which now has the form:

$$G^{\bar{p}}_{uu}(z) = G^{\bar{p}}_{ud}(z) = a_{\bar{N}} \cdot (1-z)^{\lambda - \alpha_R + 4(1-\alpha_B)} \cdot (1+3z) \,, \tag{29}$$

with a smaller value of $a_{\bar{N}}$, $a_{\bar{N}} = 0.13$, and an additional factor $(1+3z)$ with respect to the expression in ref. [10]. For all other quark distributions and fragmentation functions the same expressions as in ref. [10] have been taken. The quality of the description of the $\bar{p}$ inclusive spectra with fragmentation function of Eq. (29) is shown

to be even better than in previous papers (see Fig. 12). Here, however, the calculated inclusive density of antiprotons at RHIC energy decreases in comparison with the value presented in Table 5.

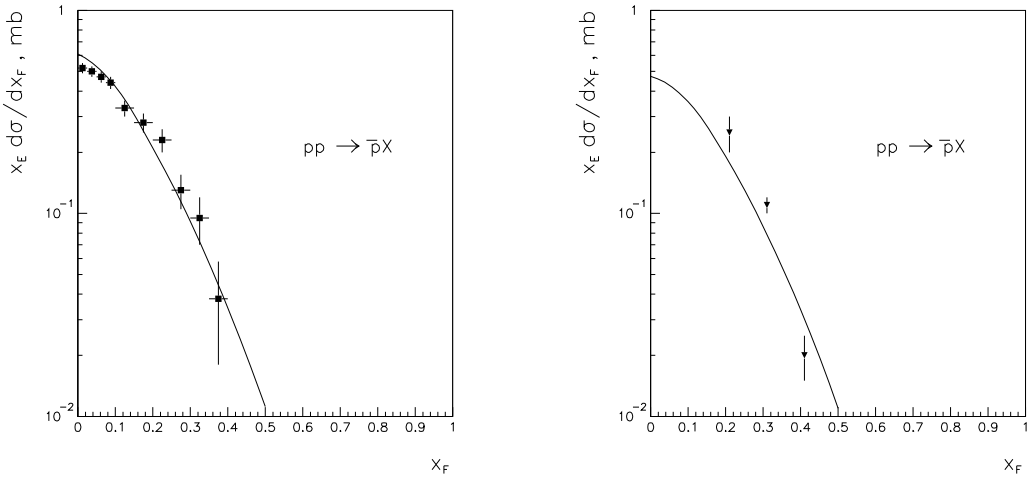


Figure 12: The experimental spectra of $\bar{p}$ produced in $pp$ collisions at 400 GeV/c [33] (left panel) and 175 GeV/c [60] (right panel), together with their QGSM description.

The ratio of $p$ to $\bar{p}$ yields at $y^* = 0$ calculated with the QGSM and with the fragmentation function in Eq. (29) is shown in the left panel of Fig. 13. The results with $\alpha_{SJ} = 0.9$ and $\varepsilon = 0.024$, $\alpha_{SJ} = 0.6$ and $\varepsilon = 0.057$, and $\alpha_{SJ} = 0.5$ and $\varepsilon = 0.0757$ are presented by dashed ($\chi^2$/ndf=21.7/10), dotted ($\chi^2$/ndf=12.2/10), and dash-dotted ($\chi^2$/ndf=11.1/10) curves, respectively. Thus the most probable value of $\alpha_{SJ}$ from the point of view of $\chi^2$ analyses is $\alpha_{SJ} = 0.5 \pm 0.1$.

The calculated ratios of $\bar{p}$ to $p$ yields as function of rapidity are shown in the right panel of Fig. 12. In accordance with the experimental conditions [34] we use here the value $\langle p_T \rangle = 0.9$ GeV/c both for secondary $p$ and $\bar{p}$. We also present here the calculations with $\alpha_{SJ} = 0.9$ and $\varepsilon = 0.024$, $\alpha_{SJ} = 0.6$ and $\varepsilon = 0.057$, and $\alpha_{SJ} = 0.5$ and $\varepsilon = 0.0757$ by dashed ($\chi^2$/ndf=72.8/10), dotted ($\chi^2$/ndf=18.6/10), and dash-dotted ($\chi^2$/ndf=17.0/10) curves, the most probable value of $\alpha_{SJ}$ being again $0.5 \pm 0.1$.

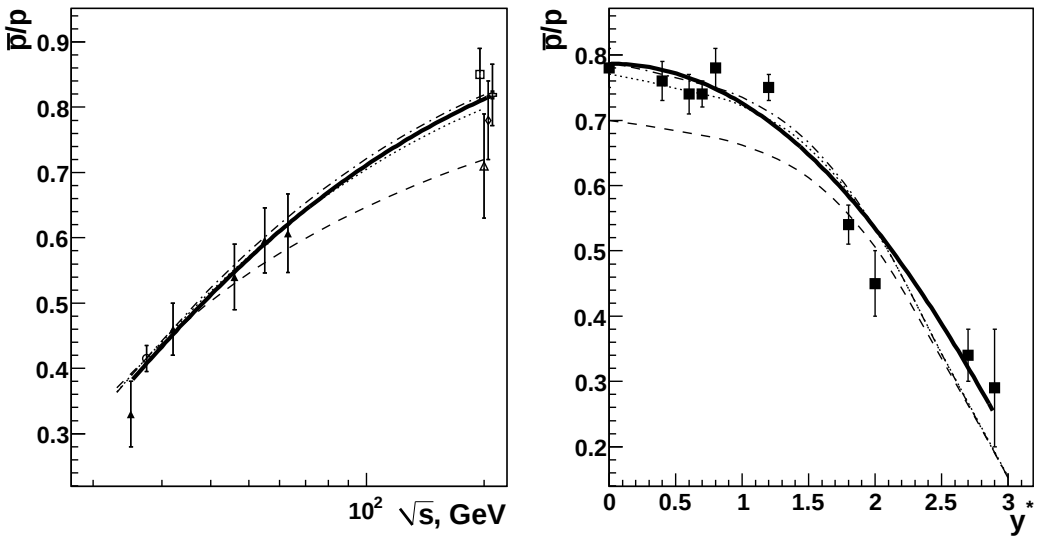


Figure 13: The experimental ratios of $\bar{p}$ to $p$ production cross sections in high energies $pp$ collisions at $y^* = 0$ [32, 33, 34, 35, 36, 37] (left panel) and as the functions of rapidity at $\sqrt{s} = 200$ GeV [34] (right panel), together with their fits by Eqs. (12), (13), and (14) (solid curves), and by the QGSM description (dashed, dotted, and dash-dotted curves).

# 8 Predictions for LHC

We present in Tables 6 and 7 our predictions for antibaryon/baryon ratios in midrapidity region at energies $\sqrt{s} = 900$ GeV and $\sqrt{s} = 14$ TeV by considering three different scenarios for the SJ contribution: not SJ contribution ($\varepsilon = 0$), SJ contribution with $\alpha_{SJ} = 0.5$, and SJ contribution with $\alpha_{SJ} = 0.9$.

The first remarkable feature of our prediction is that practically equal $\bar{B}/B$ ratios are predicted for baryons with different strangeness content, the small differences presented in Tables 6 and 7 being inside the of the accuracy of our calculations.

At $\sqrt{s} = 900$ GeV, probably the lowest energy used for testing at LHC as intermediate energy between RHIC and LHC energies, we expect the values of $\bar{B}/B$ ratios to be about 0.96 in the case of $\alpha_{SJ} = 0.5$ (which corresponds to the well known $\omega$-reggeon exchage at lower energies), and of about 0.90 in the case of $\alpha_{SJ} = 0.9$ (Odderon contribution).

| Ratio | $\sqrt{s} = 900$ GeV | | |
|---|---|---|---|
| | $\varepsilon = 0$ | $\alpha_{SJ} = 0.5$ | $\alpha_{SJ} = 0.9$ |
| $\overline{p}/p$ | 0.981 | 0.955 | 0.892 |
| $\overline{\Lambda}/\Lambda$ | 0.976 | 0.949 | 0.887 |
| $\overline{\Xi}^+/\Xi^-$ | 0.992 | 0.965 | 0.909 |
| $\overline{\Omega}^+/\Omega^-$ | 1.0 | 0.965 | 0.907 |

Table 6: The QGSM predictions for antibaryon/baryon yields ratios in $pp$ collisions in midrapidity region ($|y| < 0.5$) at $\sqrt{s} = 900$ GeV. Three different scenarios for the SJ contribution are considered: not SJ contribution ($\varepsilon = 0$), SJ contribution with $\alpha_{SJ} = 0.5$ ($\omega$-reggeon exchange), and SJ contribution with $\alpha_{SJ} = 0.9$ (Odderon exchange).

For $\sqrt{s} = 14$ TeV the $\bar{B}/B$ ratios are predicted to be larger than 0.99 for $\alpha_{SJ} = 0.5$ and of about 0.96 for $\alpha_{SJ} = 0.9$, so an experimental accuracy of the order of $\sim 1$ % in the measurement of these ratios will be needed to discriminate between the two values of $\alpha_{SJ}$.

| Ratio | $\sqrt{s} = 14$ TeV | | |
|---|---|---|---|
| | $\varepsilon = 0$ | $\alpha_{SJ} = 0.5$ | $\alpha_{SJ} = 0.9$ |
| $\overline{p}/p$ | 0.998 | 0.994 | 0.957 |
| $\overline{\Lambda}/\Lambda$ | 0.992 | 0.993 | 0.957 |
| $\overline{\Xi}^+/\Xi^-$ | 0.999 | 0.995 | 0.966 |
| $\overline{\Omega}^+/\Omega^-$ | 1.0 | 0.995 | 0.967 |

Table 7: The QGSM predictions for antibaryon/baryon yields ratios in $pp$ collisions in midrapidity region ($|y| < 0.5$) at $\sqrt{s} = 14$ TeV. Three different scenarios for the SJ contribution are considered: not SJ contribution ($\varepsilon = 0$), SJ contribution with $\alpha_{SJ} = 0.5$ ($\omega$-reggeon exchange), and SJ contribution with $\alpha_{SJ} = 0.9$ (Odderon exchange).

Our predictions for the $\bar{B}/B$ ratios at intermediate LHC energies $\sqrt{s} = 5.5$ TeV and $\sqrt{s} = 10$ TeV, calculated with Odderon contribution $\alpha_{SJ} = 0.9$, are presented in Table 8.

| Ratio | $\sqrt{s} = 5.5$ TeV | $\sqrt{s} = 10$ TeV |
|---|---|---|
| $\overline{p}/p$ | 0.942 | 0.953 |
| $\overline{\Lambda}/\Lambda$ | 0.941 | 0.953 |
| $\overline{\Xi}^+/\Xi^-$ | 0.954 | 0.962 |
| $\overline{\Omega}^+/\Omega^-$ | 0.954 | 0.962 |

Table 8: The QGSM predictions for antibaryon/baryon yields ratios in $pp$ collisions in midrapidity region ($|y| < 0.5$) for energies $\sqrt{s} = 5.5$ TeV and $\sqrt{s} = 10$ TeV, obtained by considering one Odderon contribution with $\alpha_{SJ} = 0.9$.

The midrapidity densities of produced secondaries are more model dependent than the antiparticle/particle ratios. We present in Table 9 the QGSM predictions at LHC energies $\sqrt{s} = 5.5$ TeV, $\sqrt{s} = 10$ TeV, and $\sqrt{s} = 14$ TeV, obtained by considering one Odderon contribution with $\alpha_{SJ} = 0.9$ and $\varepsilon = 0.024$. Baryon densities estimated without any Odderon contribution are smaller, and they practically coincide with the antibaryon densities at the same energy.

| Particle | $\sqrt{s} = 5.5$ TeV | $\sqrt{s} = 10$ TeV | LHC ($\sqrt{s} = 14$ TeV) |
|---|---|---|---|
| $\pi^+$ | 2.23 | 2.43 | 2.54 |
| $\pi^-$ | 2.23 | 2.43 | 2.54 |
| $K^+$ | 0.22 | 0.24 | 0.25 |
| $K^-$ | 0.22 | 0.24 | 0.25 |
| $p$ | 0.161 | 0.176 | 0.185 |
| $\overline{p}$ | 0.152 | 0.168 | 0.177 |
| $\Lambda$ | 0.0784 | 0.0868 | 0.0914 |
| $\overline{\Lambda}$ | 0.0738 | 0.0827 | 0.0875 |
| $\Xi^-$ | 0.0094 | 0.0106 | 0.0113 |
| $\overline{\Xi^+}$ | 0.0089 | 0.0102 | 0.0109 |
| $\Omega^-$ | 0.00076 | 0.00088 | 0.00094 |
| $\overline{\Omega^+}$ | 0.00073 | 0.000845 | 0.000912 |

Table 9: The QGSM results for midrapidity yields $dn/dy$ ($|y| < 0.5$) of different secondaries at LHC energies $\sqrt{s} = 5.5$ TeV, $\sqrt{s} = 10$ TeV, and $\sqrt{s} = 14$ TeV, obtained by considering one Odderon contribution with $\alpha_{SJ} = 0.9$.

# 9 Discussion and conclusions

From the general point of view, our approach, in which the Odderon effects in soft interactions are generated by $t$-channel SJ exchange, coincides with those in Refs. [1, 45, 46, 47, 52, 61]. Really, the two-Pomeron diagram in Fig. 4a leads by definition to equal yields of baryons and antibaryons in the central region, because the Pomeron has vacuum quantum numbers. All the difference in the production of baryons and antibaryons has to come from the diagrams Figs. 4b and/or 4c, where the Reggeon $R$ has negative C-parity and negative signature, so it contributes to the baryon and antibaryon production with opposite signs. In string models, such contribution is identified with SJ diffusion in rapidity space in the inelastic amplitude of particle production, and, due to unitarity, these squared inelastic amplitudes result in the diagrams of Figs. 4b, or 4c. If $\alpha_{SJ} \leq 0.6$ the $R$-reggeon with negative signature should be identified to the $\omega$-Reggeon, while in the case of $\alpha_{SJ} \geq 0.7 - 0.8$ it should be correspond to the Odderon. From this point of view, the hard Odderon represents the triple-gluon exchange [1, 52, 61], whereas the soft Odderon consists of a SJ-antiSJ exchange.

Some differences between our the numerical results and those presented in [1, 45, 46, 47, 52, 61] can be connected to the processes (diagrams) which are considered in the calculations by each approach, and to the values of the corresponding model parameters. Also, the values of $\alpha_{SJ}(0)$ extracted from the experimental data depend on the energy region and on the experimental points included into the analysis.

We neglect the possibility of interactions between Pomerons (the so-called enhancement diagrams) in our calculations. Such interactions are already very important in the cases of heavy ion [62] and nucleon-nucleus [63] collisions at RHIC energies, and their contribution should increase with energy. However, we estimate that the inclusive density of secondaries produced in $pp$ collisions at LHC energies is not large enough to affected by these effects.

In the case of heavy ion collisions, the effects of SJ diffusion ($\bar{B}B$ asymmetry and others) could be increased by the contribution to the inclusive spectrum of a secondary baryon of diagrams in which several incident nucleons interact with the target to the inclusive spectrum of a secondary baryon. The detailed study of this contribution will be a requirement of further analysis.

The experimental data on the differences in particle and antiparticle total cross sections with a proton target have been considered in Section 2. As discussed there, a possible Odderon contribution can be present in this case of $\bar{p}p$ and $pp$ total cross sections, while such an Odderon contribution shoud turn out to be zero for meson-

proton total cross sections. With the Odderon corresponding to a reggeized three-gluon exchange in $t$-channel this last feature naturally appears.

However one has to note that the possibility of an Odderon exchange contribution in $\bar{p}p$ and $pp$ is supported by the data of $\bar{p}/p$ scattering obtained at ISR energies ($\sqrt{s} \geq 30$ GeV), where experimental data (at so high energies) do not exist for $K^{\pm}p$ and $\pi^{\pm}p$ exist.

On the other hand, the main part of experimental data for the ratios of real/imaginary parts of elastic $pp$ amplitude, including the ISR data, are in agreement, either with the absence of any Odderon contribution, or with the presence of a very small Odderon contribution, if the value of $\alpha_{Odd}$ is close to one. The exceptions to this fact are the FNAL data [26] and the oldest CERN-SPS experimental point [27] that allows some room for the Odderon contribution to be present.

Thus it seems that the ISR data on the differences of particle and antiparticle total interaction cross sections and the data on the ratios of real/imaginary parts of elastic $pp$ amplitude are not completely consistent with each other.

In the case of the inclusive production of particles and antiparticles in central (midrapidity) region in $pp$ collisions we could not see any contribution by the Odderon. All experimental data starting from those at fixed target energies are consistent with a value $\alpha_R(0) \simeq 0.5$, a little larger than the conventional value of $\alpha_\omega(0) \simeq 0.4$, but still too small for the Odderon contribution to be there. On top of that, even at RHIC energies the available energy for the possible Odderon exchange is $\sqrt{s} \simeq 15{-}20$ GeV, what is perhaps too small, since we did not saw any Odderon contribution at such energies in the case of the differences of particle and antiparticle total interaction cross sections. Actually, the only evidence for the Odderon exchange with $\alpha_{Odd}(0) \simeq 0.9$ in inclusive reactions are two experimental points for $\bar{B}B$ production asymmetry by the H1 Collaboration [53, 58]. The first point [53] (for $\bar{p}/p$ ratio) is until now not published, and the second one [58] (for $\bar{\Lambda}/\Lambda$ ratio) shows a very large error bar, but, on the other hand, only for these two points the kinematics would allow the energy of the Odderon exchange to be large enough, $\sqrt{s} \simeq 100$ GeV.

One has to expect that the LHC data will make the situation more clear. The QGSM predictions for the deviation of $\bar{B}/B$ ratios from unity due to SJ contribution with $\alpha_{SJ}(0) \simeq 0.9$ have been already published [15] (see also Tables 6, 7, 8, and 9 in section 8), and they allow deviations from unity on the level of $\sim 4\%$ at $\sqrt{s} = 14$ TeV, while for smaller values of $\alpha_{SJ}(0)$ these ratios should be close to one.

**Acknowledgements**

We are grateful to A.B. Kaidalov for the idea of providing this analysis and discussions, and to Ya.I. Azimov and M.G. Ryskin for useful discussions and comments. We also thank Y. Foka and P. Christakoglou for sharing with us their insight on the experimental requirements and conditions at LHC.

This paper was supported by Ministerio de Educación y Ciencia of Spain under the Spanish Consolider-Ingenio 2010 Programme CPAN (CSD2007-00042) and project FPA 2005–01963, by Xunta de Galicia and, in part, by grants RFBR-07-02-00023 and RSGSS-1124.2003.2.

# References

[1] J. Bartels, L.N. Lipatov, and G.P. Vacca, Phys. Lett. **B477**, 178 (2000) and hep-ph/9912423.

[2] B. Nicolescu, 0707.2923 [hep-ph].

[3] H.G. Dosch, C. Ewerz, and V. Schatz, Eur. Phys. J. **C24**, 561 (2002) and hep-ph/0201294.

[4] A.P. Contogouris, L.L. Jenkovsky, E.S. Martynov, and B.V. Struminsky, Phys. Lett. **B298**, 432 (1993).

[5] S.J. Brodsky, C. Merino, and J. Rathsman, Phys. Lett. **B461**, 114 (1999) and hep-ph/9904280.

[6] P. Hägler, B. Pire, L. Szymanowski, and O.V. Teryaev, Phys. Lett. **B535**, 117 (2002).

[7] I.F. Ginzburg, I.P. Ivanov, N.N. Nikolaev, Eur. Phys. J. **C5**, 02 (2003).

[8] A. Breakstone et al., Phys. Rev. Lett. **54**, 2180 (1985).

[9] L.L. Jenkovsky, B.V. Struminsky, and A.N. Shelkovenko, Yad. Fiz. **46**, 1200 (1987).

[10] G.H. Arakelyan, A. Capella, A.B. Kaidalov, and Yu.M. Shabelski, Eur. Phys. J. **C26**, 81 (2002) and hep-ph/0103337.

[11] F. Bopp and Yu.M. Shabelski, Yad. Fiz. **68**, 2155 (2005) and hep-ph/0406158; Eur. Phys. J. **A28**, 237 (2006) and hep-ph/0603193.

[12] G.H. Arakelyan, C. Merino, and Yu.M. Shabelski, Yad. Fiz. **69**, 911 (2006) and hep-ph/0505100;
Phys. Atom. Nucl. **70**, 1110 (2007) and hep-ph/0604103;
Eur. Phys. J. **A31**, 519 (2007) and hep-ph/0610264.

[13] O.I. Piskounova, Phys. Atom. Nucl. **70**, 1110 (2007) and hep-ph/0604157.

[14] Yu.M. Shabelski, Lecture given at the XL PNPI Winter School on Physics and at the $12^{th}$ School on Theoretical Physics, St.Petersburg, Russia, February 2006, and hep-ph/0705.0947.

[15] G.H. Arakelyan, C. Merino, and Yu.M. Shabelski, Eur. Phys. J. **C54**, 577 (2008) and hep-ph/0709.3174.

[16] C. Merino, M.M. Ryzhinski, and Yu.M. Shabelski, arXiv:0810.1275[hep-ph].

[17] P.E. Volkovitsky, A.M. Lapidus, V.I. Lisin, and K.A. Ter-Martirosyan, Yad. Fiz. **24**, 1237 (1976).

[18] A. Shaale and Yu.M. Shabelski, Yad. Fiz. **46**, 594 (1987).

[19] V. Flaminio et al., Compilation of Cross Sections III: $p$ and $\bar{p}$ Induced Reactions, CERN-HERA 84-01 (1984).

[20] G. Carboni et al., Nucl. Phys.**B254**, 697 (1985).

[21] A. Donnachie and P.V. Landshoff, Phys. Lett. **B296**, 227 (1992).

[22] J.P. Burq et al., Nucl. Phys. **B217**, 285 (1983).

[23] U. Amaldi, Phys. Lett. **B66**, 390 (1977).

[24] W. Grein, Nucl. Phys. **B131**, 255 (1977).

[25] C. Auger et al., UA4/2 Collaboration, Phys. Lett. **B316**, 448 (1993).

[26] L.A. Fajardo et al., Phys. Rev. **D24**, 46 (1981).

[27] P. Bernard et al., UA4 Collaboration, Phys. Lett. **B198**, 538 (1987).

[28] R.J.M. Colovan et al., Z. Phys. **C58**, 109 (1993).

[29] A. Donnachie and P.V. Landshoff, Nucl. Phys. **B244**, 322 (1984).

[30] V.A. Abramovsky, O.V. Kancheli, and I.D. Mandzhavidze, Yad. Fiz. **13**, 1102 (1971).

[31] K.A. Ter-Martirosyan, Nucl. Phys. **B68**, 591 (1965).

[32] K. Guettler et al., Nucl. Phys. **B116**, 77 (1976).

[33] M. Aguilar-Benítez et al., Z. Phys. **C50**, 405 (1991).

[34] I.G. Bearden et al., BRAHMS Collaboration, Phys. Lett. **B607**, 42 (2005) and nucl-ex/0409002.

[35] B.B. Back et al., PHOBOS Collaboration, Phys. Rev. **C71**, 021901 (2005) and nucl-ex/0409003.

[36] S.S. Adler et al., PHENIX Collaboration, Phys. Rev. **C74**, 024904 (2006) and nucl-ex/0603010.

[37] B.I. Abelev et al., STAR Collaboration, Phys. Lett. **B637**, 161 (2006) and nucl-ex/0601033; arXiv:0808.2041 [nucl-ex].

[38] D. Ouerdane for the BRAHMS Collaboration, Proceedings of the $17^{th}$ International Conference on Ultra Reltivistic Nucleus-Nucleus Collisions (Quark Matter 2004), ed. by H.G. Ritter. X.-N. Wang, Oakland, California, 11-17 January 2004, J. Phys. **G30**:S1129-S1132 (2004), and nucl-ex/0403049.

[39] A.B. Kaidalov and K.A. Ter-Martirosyan, Yad. Fiz. **39**, 1545 (1984); **40**, 211 (1984).

[40] A.B. Kaidalov and O.I. Piskounova, Yad. Fiz. **41**, 1278 (1985); Z. Phys. **C30**,145 (1986).

[41] Yu.M. Shabelski, Yad. Fiz. **44**, 186 (1986).

[42] V.A. Abramovsky, V.N. Gribov, and O.V. Kancheli, Yad. Fiz. **18**, 595 (1973).

[43] A.B. Kaidalov, Sov. J. Nucl. Phys. **45**, 902 (1987) and Yad. Fiz. **43**, 1282 (1986).

[44] X. Artru, Nucl. Phys. **B85**, 442 (1975).

[45] M. Imachi, S. Otsuki, and F. Toyoda, Prog. Theor. Phys. **52**, 346 (1974); **54**, 280 (1976); **55**, 551 (1976).

[46] G.C. Rossi and G. Veneziano, Nucl. Phys. **B123**, 507 (1977).

[47] D. Kharzeev, Phys. Lett. **B378**, 238 (1996).

[48] V.G. Bornyanov et al., Uspekhi Fiz. Nauk. **174**, 19 (2004).

[49] D. Diakonov, V. Petrov, and M. Polyakov, Z. Phys. **A359**, 305 (1997).

[50] M.G. Ryskin and Yu.M. Shabelski, Eur. Phys. J. **C50**, 81 (2007) and hep-ph/0609222.

[51] S.E. Vance, M. Gyulassy, and X-N. Wang, Phys. Lett. **B443**, 45 (1998).

[52] B.Z. Kopeliovich and B. Povh, Z. Phys. **C75**, 693 (1997); Phys. Lett. **B446**, 321 (1999).

[53] C. Adloff et al., H1 Collaboration, Proceedings of the 29th International Conference on High Energy Physics (ICHEP98), Vancouver, Canada, July 1998.

[54] F. Bopp, hep-ph/0002190; hep-ph/0007229.

[55] A. Capella and B.Z. Kopeliovich, Phys. Lett. **B381** 325 (1996).

[56] V.V. Anisovich and V.M. Shekhter, Nucl. Phys. **B55**, 455 (1973).

[57] A. Capella and C.A. Salgado, Phys. Rev. **C60**, 054906 (1999).

[58] C. Adloff et al., H1 Collaboration, Z. Phys. **C76**, 213 (1997) and hep-ex/9705018.

[59] B.I. Abelev et al., STAR Collaboration, Phys. Rev. **C75**, 064901 (2007) and nucl-ex/0607033.

[60] A.E. Brenner et al., Phys. Rev. **D26** 1497 (1982).

[61] B.Z. Kopeliovich and B.G. Zakharov, Phys. Lett. **B211**, 221 (1988); Sov. J. Nucl. Phys. **48**, 136 (1988); Z. Phys. **C43**, 241 (1989).

[62] A. Capella, A Kaidalov, and J. Tran Thanh Van, Heavy Ion Phys. **9**, 169 (1999).

[63] C. Merino, C. Pajares, and Yu.M. Shabelski, Eur. Phys. J. **C59**, 691 (2009) and arXiv:0802.2195[hep-ph].